



INSTITUT DE FRANCE
Académie des sciences

Comptes Rendus

Mécanique


Quentin Marcot, Thomas Fourest, Bertrand Langrand and Fabrice Pierron

The Laplace Virtual Fields Method for the direct extraction of viscoelastic properties of materials

Volume 351 (2023), p. 171-199

Published online: 12 May 2023

<https://doi.org/10.5802/crmeca.181>

 This article is licensed under the
CREATIVE COMMONS ATTRIBUTION 4.0 INTERNATIONAL LICENSE.
<http://creativecommons.org/licenses/by/4.0/>



*Les Comptes Rendus. Mécanique sont membres du
Centre Mersenne pour l'édition scientifique ouverte*

www.centre-mersenne.org

e-ISSN : 1873-7234



Spontaneous articles / *Articles spontanés*

The Laplace Virtual Fields Method for the direct extraction of viscoelastic properties of materials

Quentin Marcot^{*, a, b}, Thomas Fourest^{® a}, Bertrand Langrand^{® a, b}
and Fabrice Pierron^{® c, d}

^a DMAS, ONERA, F-59014, Lille, France

^b Univ. Polytechnique Hauts-de-France, LAMIH, UMR CNRS 8201, F-59313 Valenciennes, France

^c Faculty of Engineering & Physical Sciences - University of Southampton, Highfield Road SO171BJ, Southampton - UK

^d MatchID NV, Leiekaai 25A, 9000 Ghent - Belgium

E-mails: quentin.marcot@onera.fr (Q. Marcot), thomas.fourest@onera.fr (T. Fourest), bertrand.langrand@onera.fr (B. Langrand), F.Pierron@soton.ac.uk (F. Pierron)

Abstract. This work proposes a new method aiming at the direct identification of viscoelastic properties of materials with a Laplace formalism implemented in the Virtual Fields Method and named L-VFM. Using a single test, this formalism allows for a direct extraction of the different viscoelastic properties without any parametric description of their time dependency. The Laplace transform enables the use of theory of elasticity in the Laplace domain. The constitutive equations are expressed in the plane stress framework with the 2D plane stress stiffness coefficients. The conversion from the 2D plane stress stiffness coefficients to the bulk and shear moduli as well as Poisson's ratio and Young's modulus is realised in the Laplace domain. The inverse Laplace transform is then applied to these functions in order to obtain the temporal evolution of the material properties. The L-VFM changes the viscoelastic identification from a non-linear to a linear process.

Keywords. Identification, Virtual Fields Method, Linear viscoelasticity, Laplace transform, Inverse Laplace transform.

Funding. The first author is supported by the French Ministry of Defense (AID) for this work.

Manuscript received 2 September 2022, revised 5 December 2022 and 31 January 2023, accepted 15 February 2023.

* Corresponding author.

1. Introduction

As new materials, design and optimization tools are constantly being developed, certification programs in the aerospace industry tends toward an increasing reliance on modelling and simulations for the reduction of physical testing. In the particular case of materials and structures, this virtual certification process is generally supported by a validation stage which will determine the ability of a model to fit experimental data. For this, model calibration tests must be performed where the model parameters are adjusted in order to fit data sets generated for different experimental conditions. In order to widen the range of validity of the given model parameters, these tests must be performed to cover a wide range of observable quantities such as strains, strain rates, temperature, etc.

In the case of viscoelastic materials, the properties can be determined using standard tests such as creep tests [1], dynamic mechanical analysis (DMA) [2] or standard tensile tests [3]. However, these tests are limited to the characterisation of only one relaxation function at a time. As stated in [4], the complete characterisation of the viscolastic behaviour for an isotropic material can be obtained with the determination of two viscoelastic response functions simultaneously, this is known as the Standard Protocol. With the recent improvements in imaging, non-invasive full-field measurement techniques have been developed giving access to maps of observable quantities. For kinematic field measurements, Digital Images Correlation (DIC) has been widely used [5]. In particular, it enabled the emergence of new methods to identify isotropic viscoelastic properties. One set of such methods uses DIC together with data generated from standard tests, allowing to identify simultaneously the Young's modulus and Poisson's ratio by measuring the longitudinal and lateral strains [6–8]. These techniques take advantages of the non-contact nature of DIC to avoid experimental difficulties arising from the use of strain gauges such as alignment, stiffness of the backing (which must be lower than the tested polymer) or inadequate temperature compensation.

However, these methods use statically determinate test configurations, which strongly limits test geometry and rely on strong assumptions on boundary conditions. Thus, there is a growing interest in using statically undetermined approaches for the identification of constitutive parameters of materials. These methods take advantage of heterogeneous stress fields for the identification procedure which gives the potential to widen the range of validity of the identified parameters using a reduced number of tests [9, 10]. This new testing paradigm has recently been coined Material Testing 2.0 [11]. The price to pay for using statically indeterminate test configurations however is that there is no direct link between the measured external forces applied to the specimen and the local strain response. Therefore, an inverse identification methodology needs to be employed [9]. Among those methods, the Virtual Fields Method (VFM) is a good candidate. The VFM uses measured observables obtained with full-field measurements, and expresses the stresses via a model that depends on the nature of the tested material [12, 13]. The stresses are then used to express the principle of virtual work (PVW). The model parameters are evaluated based on the stress equilibrium described by the PVW with particular virtual fields. In the case of elasticity, the linear stress-strain relationship allows for the constitutive parameters to be directly identified using a matrix inversion [14]. If a non-linear constitutive relationship is considered, the model parameters are obtained by minimising a cost function built from the difference between internal and external virtual works. Viscoelastic materials can be formulated with rheological models, and an iterative minimisation procedure has to be employed [15, 16].

However, constitutive relationships for viscoelastic materials can be represented with an equivalent elastic formulation in the Laplace domain. This is known as the viscoelastic correspondence principle [17, 18]. This principle is widely used for the analysis of viscoelastic materials. In particular, it has been used for the conversion of viscoelastic functions using a Prony series

representation (generally from Young's modulus $E(t)$ to the creep compliance $D(t)$) [6, 19]. Other applications invoke this principle for homogenisation problems, where the effective viscoelastic properties need to be retrieved from the knowledge of the microstructure [20, 21]. More recently, Taguchi et al. [22] used this correspondence principle in order to compute viscoelastic stresses within a plane stress framework, and considering time-varying Poisson's ratio.

The present work aims at developing a Laplace formalism for the VFM via the viscoelastic correspondence principle. Since the VFM leads to a direct inversion for a purely elastic model, applying the Laplace transform to equilibrium equation allows to identify viscoelastic parameters without any iterative minimisation procedure. Using the inverse Laplace transform, the temporal description of the viscoelastic properties can be obtained without the need for an a priori parameterization. The paper is divided into three sections. Firstly, the theoretical development of the method is presented (Section 2). The data processing and tools used for the application of the method and the conversion of the viscoelastic properties are described in Section 3. The verification and performance of the proposed Laplace Virtual Fields Method (L-VFM) are addressed in Section 4 where the method is applied to Finite Element generated data with and without the introduction of noise.

2. Theoretical development

This section is devoted to the theoretical development of a Laplace formalism for the VFM. The constitutive relationships for viscoelastic materials can be written with a time domain representation and a complex frequency representation via the Laplace transform. The latter allows to use the theory of elasticity in the Laplace domain. Applying the Laplace transform to equilibrium equation expressed with the VFM allows to build up a linear system and to identify the viscoelastic stiffnesses with a direct inversion of the system in the Laplace transform domain. The temporal description of the stiffnesses can be obtained via inverse Laplace transform.

2.1. Constitutive relationships for linear viscoelastic materials

Constitutive relationships for viscoelastic materials use two descriptions. The first description, in the time domain, links the stress response to the strain history inputs by means of a convolution integral between the stiffness and strain components. The second description, in the complex frequency domain, expresses the convolution operator as a simple algebraic product between the respective Laplace transforms of the stiffness and strain components.

2.1.1. Time representation

The general linear viscoelastic constitutive relations, in the real time domain, are given by the Boltzmann superposition principle [23] such that the stress can be expressed as [24]

$$\sigma_{ij}(t) = \int_0^t C_{ijkl}(t-\tau) \dot{\epsilon}_{kl}(\tau) d\tau \quad (1)$$

where C_{ijkl} is the fourth order viscoelastic stiffness tensor, $\dot{\epsilon}_{kl}$ is the linearized strain rate tensor, with $(i,j,k,l=1,2,3)$. The dot denotes the local time derivative with respect to τ . In the case of an isotropic viscoelastic material, Equation (1) can be formulated as [18, 25]

$$\sigma_{ij}(t) = \int_0^t K(t-\tau) \dot{\epsilon}_{kk}^V(\tau) \delta_{ij} d\tau + 2 \int_0^t G(t-\tau) \dot{\epsilon}_{ij}^D(\tau) d\tau \quad (2)$$

where $K(t)$ and $G(t)$ are the bulk and shear moduli respectively, $\dot{\epsilon}_{kk}^V \delta_{ij}$ and $\dot{\epsilon}_{ij}^D$ are the volumetric and deviatoric strain rate tensors respectively.

The operators used in Equations (1) and (2) are known as the hereditary, or convolution, integrals. The stress components σ_{ij} at a given time t are a weighted average of the strain increments, $d\varepsilon_{ij} = \dot{\varepsilon}_{ij}d\tau$, by the corresponding modulus history, also called memory kernel, up to that time t . The principle of convolution is illustrated in Figure 1 for a constant uniaxial strain rate (i.e. the strain increment $\Delta\varepsilon$ is constant at each time step). The corresponding stress response is illustrated on the right side of Figure 1. Two cases are presented:

- In Figure 1a, the modulus time dependency is negligible. The stress displays a typical linear elastic response and all the strain energy caused by the mechanical load is stored within the material.
- In Figure 1b, the modulus relaxes with time. The stress displays a viscoelastic response with stress softening as the strain energy is dissipated from the relaxation mechanisms within the material.

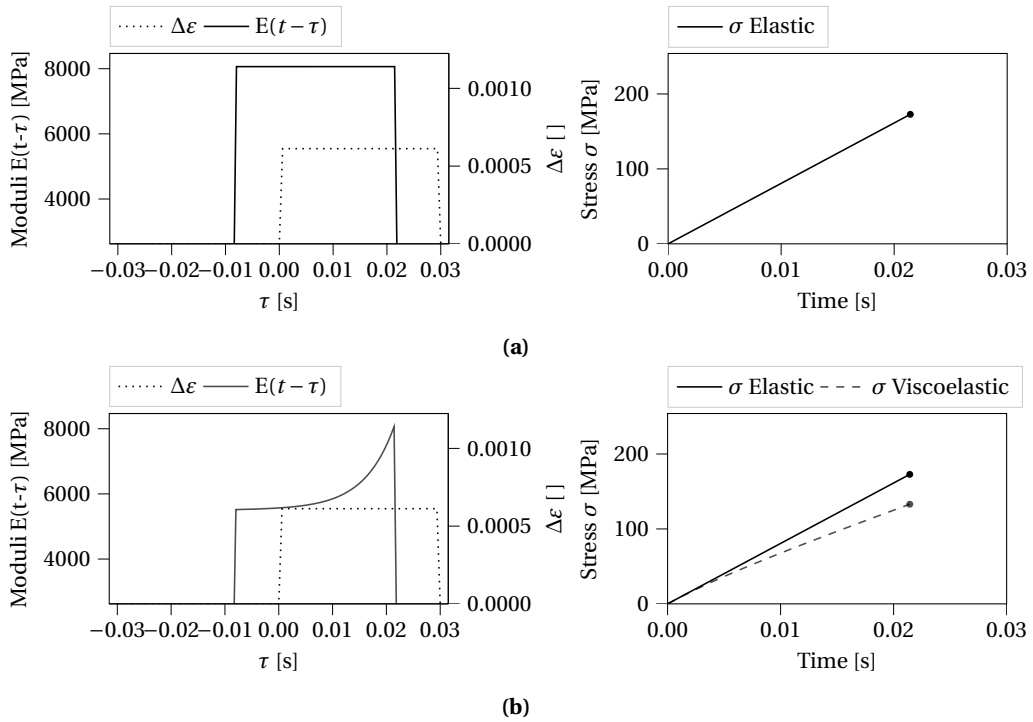


Figure 1. Convolution operation for, **(a)**, a perfectly linear elastic behaviour, the modulus (kernel) is constant with time, and the stress response is linear, **(b)**, a viscoelastic behaviour, the decrease of the modulus with time induces stress softening in the response

2.1.2. Complex frequency representation

The temporal representation of the constitutive relationships given by Equations (1) and (2) can be reformulated with integral transform methods. In this framework, the most suited transform is the well-known unilateral Laplace transform [26], which maps a time domain function into the complex frequency domain. It is defined as

$$F(s) = \mathcal{L}\{f(t)\}(s) := \int_0^{\infty} f(t) \exp(-st) dt \quad (3)$$

where \mathcal{L} denotes the Laplace transform symbol, s is the complex valued variable associated with the transform such that $s = \zeta + i\omega$ with ζ , the real part, ω , the imaginary part with $i = \sqrt{-1}$, the term $\exp(-st)$ is the integration kernel. $F(s)$ is the transform of the function $f(t)$. Functions defined in the Laplace domain can be converted to the time domain using the inverse Laplace transform, \mathcal{L}^{-1} , generally defined with the Bromwich contour integral [27] given by

$$f(t) = \mathcal{L}^{-1}\{F(s)\}(t) = \frac{1}{2\pi i} \int_{\zeta-i\infty}^{\zeta+i\infty} F(s) \exp(st) ds \quad (4)$$

The interest of the Laplace transform lies in the fact that some of its properties allow for an easier manipulation of mathematical operators of the time domain in the complex frequency domain. A first such property is the *convolution theorem*, which states that the convolution of two functions in the time domain is equivalent to the product of their respective Laplace transforms in the complex frequency domain as expressed in Equation (5)

$$\mathcal{L}\left\{\int_0^t f(t-\tau)g(\tau)d\tau\right\} = \mathcal{L}\{f \otimes g\}(t) = F(s)G(s) \quad (5)$$

where \otimes is the convolution operator, $F(s)$ and $G(s)$ are the Laplace transforms of the functions $f(t)$ and $g(t)$ respectively. Another property of the Laplace transform concerns time derivatives. A differential equation in the real time domain is equivalent to an algebraic equation in the transform domain, given $g(t) = \frac{dh(t)}{dt} = \dot{h}(t)$, the Laplace transform of $g(t)$ is written as

$$\mathcal{L}\{g(t)\} = \mathcal{L}\left\{\frac{dh(t)}{dt}\right\} = sH(s) - h(0) \quad (6)$$

where $h(0)$ is the initial condition of the function $h(t)$ and $H(s)$ is the Laplace transform of $h(t)$.

Considering these two properties and applying the Laplace transform to Equation (2), with the assumption that the strains vanish at $t \leq 0$, the general relationship becomes

$$\sigma_{ij}(s) = sC_{ijkl}(s)\varepsilon_{kl}(s) \quad (7)$$

and for an isotropic material,

$$\sigma_{ij}(s) = sK(s)\varepsilon_{kk}^V\delta_{ij}(s) + 2sG(s)\varepsilon_{ij}^D(s) \quad (8)$$

The last expressions describes the so-called *viscoelastic correspondence principle*¹ [18,28]. This principle states that the viscoelastic stress model given by Equations (1) and (2) are equivalent to an elastic stress model in the Laplace domain (Equations (7) and (8)).

In the case of a harmonic excitation, such as with DMA, the Fourier transform could have been used. This is because the Fourier transform of a signal is equivalent to its Laplace transform evaluated for $s = i\omega$. Assuming that $\zeta = 0$ is equivalent to assume that no transient effect occurs during the test. In the case of a transient analysis, the Laplace transform is well suited as it allows to capture transient as well as steady state behaviours.

2.2. The Virtual Fields Method

The VFM is an identification technique based on the principle of virtual work. The VFM is used for the identification of constitutive relationships of materials using heterogeneous data obtained via full-field measurements [12, 13]. The underpinning idea is to generate the largest stress heterogeneities for a wider validity of the constitutive parameters with a reduced number of tests. The VFM can be applied to any kind of behaviour. It has been used to identify elastic [14], plastic [29], viscoplastic [30], anisotropic [31,32] and viscoelastic [15,33] material models, among others.

¹These expressions are more generally known as the Laplace-Carson transform of the constitutive relationships, however, the Laplace transform denomination will be used here

2.2.1. General framework

For quasi-static loading conditions, the principle of virtual works is expressed as

$$\underbrace{\int_V \underline{\underline{\sigma}}(\underline{X}, t, \varepsilon, T, \dots) : \underline{\underline{\varepsilon}}^* dV}_{W_{int}^*(\underline{X}, t)} - \underbrace{\int_{\partial V} \underline{T}(t) \cdot \underline{u}^* dS}_{W_{ext}^*(t)} = 0 \quad (9)$$

where V is the volume of the considered solid, ∂V is its smooth, or piecewise-smooth boundary, $\underline{\underline{\sigma}}$ is the Cauchy stress tensor, \underline{T} is the traction-vector, \underline{u}^* is the virtual displacement vector and $\underline{\underline{\varepsilon}}^*$ is the virtual strain tensor. The two operators $:$ and \cdot denote the double and simple dot product respectively. Equation (9) expresses the equilibrium between the virtual work of internal forces $W_{int}^*(\underline{X})$, depending on the material parameters, and the virtual work of external forces W_{ext}^* , which represents the contribution of external loads. These two quantities are scalar values. Equation (9) is valid for any continuous (\mathcal{C}^0) and piecewise differentiable virtual displacement field. The stresses in Equation (9) are calculated by applying a constitutive law depending on observable quantities such as strains, strain rates, temperatures, etc. In practice, full-field measurements are performed at the surface of the specimen subjected to mechanical loading. To allow for the volume integrals to be calculated from surface measurements, a 2D plane stress assumption is made in most applications, which is typical for material testing.

For linear elastic constitutive models, the stress $\underline{\underline{\sigma}}$ is linearly dependant on the strains. So, Equation (9) can then be expressed in order to allow for a direct matrix inversion for the identification of elastic properties [13, 14]. This is referred to as the linear VFM. For non-linear constitutive models, the identification relies on the minimisation of a cost function Φ , deduced from Equation (9) [15, 29–33]. It describes the normalized squared residuals between the internal virtual works and external virtual works as shown in Equation (10)

$$\Phi(\underline{X}) = \sum_{t=1}^{N_t} \left[\frac{W_{ext}^*(t) - W_{int}^*(t)(\underline{X})}{W_{ext}^*(t)} \right]^2 \quad (10)$$

where \underline{X} denotes the constitutive parameters set to be identified, N_t the total number of load steps and t the actual time step. The constitutive parameters are deduced from the argument minimising the cost function. This is known as the non-linear VFM. This technique computes the stress from the constitutive model for each load step, and for each guess of the parameter set. The cost function should be sufficiently “well-behaved” to allow for the target parameters to be identified robustly, as local minima can arise from measurement noise.

2.2.2. The Virtual Fields Method for viscoelasticity

The identification of the viscoelastic properties with the non-linear VFM using a time representation requires to:

- describe the time dependance of the modulus $K(t)$ and $G(t)$;
- numerically compute the convolution integrals given by Equation (2) in a plane stress framework;
- set up the iterative process described in Equation (10) until convergence.

This process has been applied to viscoelasticity by Yoon and Siviour [15] for characterisation of rubbers. In this case a combination of an Ogden and a Prony series model was used. It was also used by Hoshino et al. [16], where the minimisation was performed using a Newton–Raphson method. More recently, Matejunas et al. [33] performed finite element simulations of an Image Based Inertial Impact test with a generalized Maxwell model. The authors addressed the ability of the non-linear VFM to identify a Prony series pair and defined a timescale of the test for which the parameter could be identified.

The following section describes a different VFM formalism for viscoelasticity. Expressing the equilibrium principle in the complex frequency domain allows for the use of the viscoelastic correspondance principle. An equivalent linear system is built to express the plane stress viscoelastic stiffness components directly in the Laplace domain. The identification procedure is reduced to the inversion of a linear system. The bulk and shear moduli as well as Poisson's ratio and Young's modulus are directly expressed from the knowledge of the plane stress stiffness components in the Laplace domain. The inverse Laplace transform is then applied to compute the modulus value at each time step. The major advantage of the proposed formalism is that it does not requires an a priori parameterization of the time-dependence of the stiffness.

2.3. Application of the Laplace transform to equilibrium equations

Equation (9) expresses the principle of virtual work in the time domain. Considering that the stress components are time dependent, $\underline{\underline{\sigma}} = \underline{\underline{\sigma}}(\underline{X}, t)$, applying the Laplace transform to Equation (9) gives

$$\mathcal{L} \left\{ \int_V \underline{\underline{\sigma}}(\underline{X}, t) : \underline{\underline{\varepsilon}}^* dV \right\} = \mathcal{L} \left\{ \int_{\partial V} \underline{T}(t) \cdot \underline{u}^* dS \right\} \quad (11)$$

Since the Laplace transform is a linear integral operator, the order of integration in Equation (11) can be changed such that

$$\int_V \mathcal{L} \left\{ \underline{\underline{\sigma}}(\underline{X}, t) : \underline{\underline{\varepsilon}}^* \right\} dV = \int_{\partial V} \mathcal{L} \left\{ \underline{T}(t) \cdot \underline{u}^* \right\} dS \quad (12)$$

To isolate the constitutive relationships, a *temporally constant virtual field* such that $\underline{u}^*(t) = \underline{u}^*$ and $\underline{\underline{\varepsilon}}^*(t) = \underline{\underline{\varepsilon}}^*$ is considered. From the linearity of the transformation, Equation (12) can be written as

$$\int_V \mathcal{L} \left\{ \underline{\underline{\sigma}}(\underline{X}, t) \right\} : \underline{\underline{\varepsilon}}^* dV = \int_{\partial V} \mathcal{L} \left\{ \underline{T}(t) \right\} \cdot \underline{u}^* dS \quad (13)$$

which can be expressed using the complex variable s ,

$$\boxed{\int_V \underline{\underline{\sigma}}(\underline{X}, s) : \underline{\underline{\varepsilon}}^* dV = \int_{\partial V} \underline{T}(s) \cdot \underline{u}^* dS} \quad (14)$$

$\underbrace{\hspace{10em}}_{W_{int}^*(\underline{X}, s)} \qquad \underbrace{\hspace{10em}}_{W_{ext}^*(s)}$

Equation (14) provides the principle of virtual work in the Laplace transform domain, for a temporally constant virtual field. The quantities $\underline{\underline{\sigma}}(\underline{X}, s)$ and $\underline{T}(s)$ are the Laplace transforms of the stress tensor and the traction vector respectively.

The Laplace transform of the stress $\underline{\underline{\sigma}}(\underline{X}, s)$ can be expressed using Equation (8), however, as stated in Section 2.2, the VFM is generally provided with measurements performed over the surface of the specimen, such that a 2D plane stress assumption is made. Since the theory of elasticity holds in the Laplace domain, the model given by Equation (8) can be expressed in the plane stress framework by Equation (15)

$$\begin{bmatrix} \sigma_{11}(s) \\ \sigma_{22}(s) \\ \sigma_{12}(s) \end{bmatrix} = s \begin{bmatrix} Q_{11}(s) & Q_{12}(s) & 0 \\ Q_{12}(s) & Q_{11}(s) & 0 \\ 0 & 0 & \frac{Q_{11}(s) - Q_{12}(s)}{2} \end{bmatrix} \begin{bmatrix} \varepsilon_{11}(s) \\ \varepsilon_{22}(s) \\ 2\varepsilon_{12}(s) \end{bmatrix} = s \underline{\underline{Q}}(s) \underline{\underline{\varepsilon}}(s) \quad (15)$$

with $Q_{11}(s)$ and $Q_{12}(s)$ the plane stress stiffness components. One should note that the Voigt notation is used in this formulation, the second order symmetric stress and strain tensors are expressed with a one dimensional tensor. The passage from Equation (8) to Equation (15) is given in Appendix A of this document.

Substituting Equation (15) into Equation (14), the problem can be expressed as

$$\int_V \underline{s} Q(s) \underline{\varepsilon}(s) \cdot \underline{\varepsilon}^* dV - \int_{\partial V} \underline{T}(s) \cdot \underline{u}^* dS = 0 \quad (16)$$

Since the kinematic fields are considered to be constant through the thickness, and considering a spatially constant thickness, Equation (16) can be simplified as

$$\int_S \underline{s} Q(s) \underline{\varepsilon}(s) \cdot \underline{\varepsilon}^* dS - \int_L \underline{T}(s) \cdot \underline{u}^* dl = 0 \quad (17)$$

with S the surface of the solid and L its boundary². Considering that the two in-plane stiffness components $Q_{11}(s)$ and $Q_{12}(s)$ are the only unknowns, two linearly independent virtual fields $\{[u_1^{*(i)} \ u_2^{*(i)}]^T; [\varepsilon_{11}^{*(i)} \ \varepsilon_{22}^{*(i)} \ 2\varepsilon_{12}^{*(i)}]^T\}$ ($i=1,2$) must be chosen. Expanding Equation (17) and assuming Q_{11} and Q_{12} are constants over the surface S , the following expression is obtained

$$\underline{s} \underbrace{\begin{bmatrix} A_{11}(s) & A_{12}(s) \\ A_{21}(s) & A_{22}(s) \end{bmatrix}}_A \underbrace{\begin{bmatrix} Q_{11}(s) \\ Q_{12}(s) \end{bmatrix}}_Q = \underbrace{\begin{bmatrix} B_1(s) \\ B_2(s) \end{bmatrix}}_B \quad (18)$$

with

$$\begin{cases} A_{i1}(s) = \int_S \left(\varepsilon_{11}(s) \varepsilon_{11}^{*(i)} + \varepsilon_{22}(s) \varepsilon_{22}^{*(i)} + 2\varepsilon_{12}(s) \varepsilon_{12}^{*(i)} \right) dS \\ A_{i2}(s) = \int_S \left(\varepsilon_{11}(s) \varepsilon_{22}^{*(i)} + \varepsilon_{22}(s) \varepsilon_{11}^{*(i)} - 2\varepsilon_{12}(s) \varepsilon_{12}^{*(i)} \right) dS \\ B_i(s) = \int_L \left(T_1(s) u_1^{*(i)} + T_2(s) u_2^{*(i)}(s) \right) dl \end{cases} \quad (19)$$

In practice, full-field measurements generally provide data (displacements, strains) over a grid of discrete points. Each point is associated with an elementary surface. For each point, the datum is considered constant over its associated elementary surface. The continuous integral $A_{i1}(s)$ and $A_{i2}(s)$ given in Equation (19) can be approximated as a sum of discrete points such that

$$\begin{cases} A_{i1}(s) = \sum_{k=1}^{N_p} \left(\varepsilon_{11}^k(s) \varepsilon_{11}^{*(i),k} + \varepsilon_{22}^k(s) \varepsilon_{22}^{*(i),k} + 2\varepsilon_{12}^k(s) \varepsilon_{12}^{*(i),k} \right) \times a_k \\ A_{i2}(s) = \sum_{k=1}^{N_p} \left(\varepsilon_{11}^k(s) \varepsilon_{22}^{*(i),k} + \varepsilon_{22}^k(s) \varepsilon_{11}^{*(i),k} - 2\varepsilon_{12}^k(s) \varepsilon_{12}^{*(i),k} \right) \times a_k \end{cases} \quad (20)$$

where k refers to the data points, N_p is the number of points, a_k is the area of the elementary surface associated with each data point. The distribution of the locals traction vectors \underline{T} is generally unknown, only the resultant is generally measured with load cells. Therefore, the virtual fields must be chosen such that the virtual displacements are constant over the boundary where the load is measured (∂V in Equation (14)). The quantity $B_i(s)$ in Equation (19) can then be written such that only the resultant load appears in the equation

$$B_i(s) = \underline{u}^{*(i)} \cdot \int_L \underline{T}(s) dl = \underline{u}^{*(i)} \cdot \underline{F}(s) \quad (21)$$

²It is important to note that the the virtual displacements acts like a filter on the whole boundary of the solid. In practice, this allows to either filter out or to determine reaction forces along a given part of the solid.

One should note that, following the linearity property of the Laplace transform, Equations (20) and (21) can be expressed as

$$\left\{ \begin{array}{l} A_{i1}(s) = \mathcal{L}\{A_{i1}(t)\} = \mathcal{L}\left\{ \sum_{k=1}^{N_p} \left(\varepsilon_{11}^k(t) \varepsilon_{11}^{*(i),k} + \varepsilon_{22}^k(t) \varepsilon_{22}^{*(i),k} + 2\varepsilon_{12}^k(t) \varepsilon_{12}^{*(i),k} \right) \times a_k \right\} \\ A_{i2}(s) = \mathcal{L}\{A_{i2}(t)\} = \mathcal{L}\left\{ \sum_{k=1}^{N_p} \left(\varepsilon_{11}^k(t) \varepsilon_{22}^{*(i),k} + \varepsilon_{22}^k(t) \varepsilon_{11}^{*(i),k} - 2\varepsilon_{12}^k(t) \varepsilon_{12}^{*(i),k} \right) \times a_k \right\} \\ B_i(s) = \mathcal{L}\{B_i(t)\} = \mathcal{L}\{\underline{u}^{*(i)} \cdot \underline{F}(t)\} \end{array} \right. \quad (22)$$

Assuming that matrix A is invertible by defining linearly independent virtual fields, the solution of the linear system deriving from Equation (18) can be symbolically expressed in the Laplace domain, which yields

$$\left[\begin{array}{c} Q_{11}(s) \\ Q_{12}(s) \end{array} \right] = \frac{1}{s} \left[\begin{array}{cc} A_{11}(s) & A_{12}(s) \\ A_{21}(s) & A_{22}(s) \end{array} \right]^{-1} \left[\begin{array}{c} B_1(s) \\ B_2(s) \end{array} \right] \quad (23)$$

Equation (23) gives the expression of the two independent plane stress stiffness components in the Laplace domain. They are computed with a direct inversion of the system from the knowledge of $A_{i1}(s)$, $A_{i2}(s)$ and $B_i(s)$. Since the theory of elasticity holds in the Laplace domain, the bulk and shear moduli $K(s)$ and $G(s)$ as well as the Poisson's ratio $\nu(s)$ can be expressed with $Q_{11}(s)$ and $Q_{12}(s)$ by [4],

$$\left\{ \begin{array}{l} \nu(s) = \frac{Q_{12}(s)}{sQ_{11}(s)} \\ E(s) = Q_{11}(s) [1 - (s\nu(s))^2] \\ K(s) = \frac{E(s)}{3[1 - 2s\nu(s)]} \\ G(s) = \frac{E(s)}{2[1 + s\nu(s)]} \end{array} \right. \quad (24)$$

The relationships given by Equation (23) and (24) show that the viscoelastic stiffness components can be directly expressed using the VFM in the complex frequency domain. The temporal description for each elastic constant can be obtained with inverse Laplace transform, from Equation (4), such that,

$$\left\{ \begin{array}{l} \nu(t) = \mathcal{L}^{-1} \left\{ \frac{Q_{12}(s)}{sQ_{11}(s)} \right\} \\ E(t) = \mathcal{L}^{-1} \{ Q_{11}(s) [1 - (s\nu(s))^2] \} \\ K(t) = \mathcal{L}^{-1} \left\{ \frac{E(s)}{3[1 - 2s\nu(s)]} \right\} \\ G(t) = \mathcal{L}^{-1} \left\{ \frac{E(s)}{2[1 + s\nu(s)]} \right\} \end{array} \right. \quad (25)$$

The developments in this section show that the viscoelastic properties can be identified directly using a Laplace formalism combined with the Virtual Fields Method. The next section aims at providing different tools for a numerical implementation of this identification method.

3. Data processing and tools

The different steps established in the theoretical section can be summarised in the flowchart given by Figure 2. The difference with the standard linear VFM is the processing of the data via Laplace and inverse Laplace transforms, as shown in the dashed grey box in Figure 2.

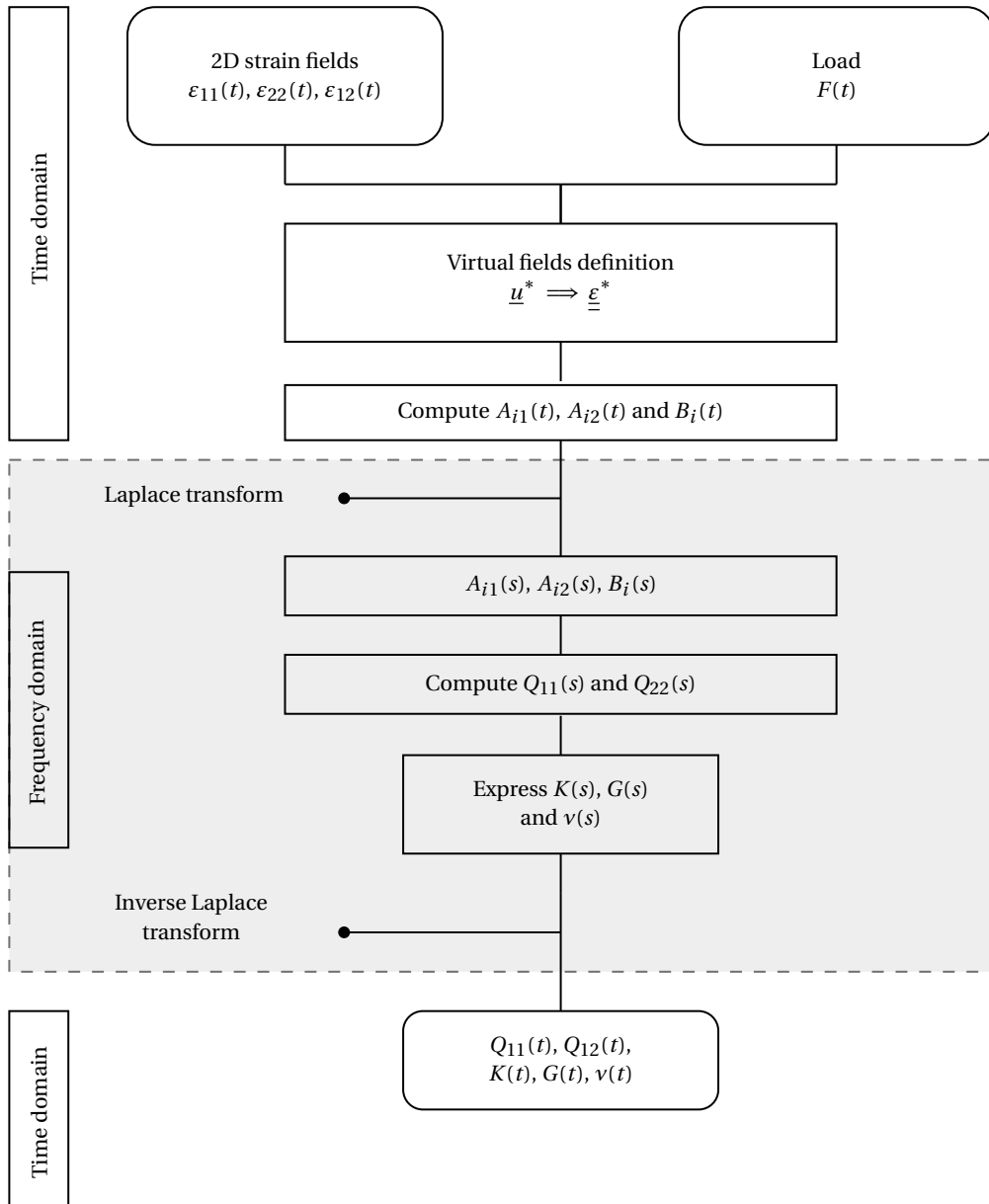


Figure 2. Flowchart of the data processing using the Laplace Virtual Fields Method

Generally, problems involving Laplace and inverse Laplace transforms can be solved analytically by using charts [34]. This is not the case here. The different quantities involved in Equation (23) are not analytically defined, such that no direct solution can be used. This sections aims at providing the tools for a numerical resolution of the problem.

3.1. Numerical Laplace and inverse Laplace transform methods

Numerical methods can be used to approximate the transform pair given by Equations (3) and (4). One set of methods approximate those integrals with a finite sum, as in [22, 35]. Another set of methods, known as the Abate–Whitt framework [36], use analytically defined Laplace transforms, and compute their inverse approximating the Bromwich formula given in Equation (4). Amongst these methods, Euler [37], Gaver [38] and Concentrated Matrix Exponential (CME) [27] methods show great potential for numerical inversion. The CME method will be considered in this paper, as it has been shown to provide greater accuracy on the numerical inversion process [27].

3.2. Processing of discrete data

In order to use a numerical inversion within the Abate–Whitt framework, an analytical expression of the Laplace transform $F(s)$ of $f(t)$ has to be defined. The expressions $A_{i1}(s)$, $A_{i2}(s)$ and $B_i(s)$ in Equation (22) are the transforms of the discrete valued data set $A_{i1}(t)$, $A_{i2}(t)$ and $B_i(t)$.

In practice, the data set could be fitted with polynomial functions, or any function which can be analytically defined in the Laplace domain [34]. Here, a linear piecewise approximation has been chosen from the work of Gómez and Uribe [39]. The method described in that paper has been modified such that the support of the piecewise function is extended to infinity to avoid computational inaccuracy (see Appendix B). This piecewise approximation can then easily be Laplace-transformed using the Laplace transform of linear and Heaviside functions [34].

3.3. Laplace inversion at time $t = 0$

Since the inverse Laplace transform is computed using the Abate–Whitt framework method, the values of the elastic constants at time $t = 0$ cannot be obtained directly (see [36]). To do so, the *initial value theorem* (IVT) will be used. This theorem states that the initial value of a function $f(t)$ can be obtained from its Laplace transform with

$$f(t = 0^+) = \lim_{s \rightarrow \infty} sF(s) \quad (26)$$

The values at time $t = 0$ can be obtained by applying this theorem to the built functional from Equation (24) for the different viscoelastic functions.

3.4. Interconversion using discrete data

The moduli $K(s)$ and $G(s)$ and Poisson's ratio $\nu(s)$ are expressed from the plane stress stiffness component $Q_{11}(s)$ and $Q_{12}(s)$. This means that the conversion is directly processed in the Laplace domain from their discrete representation. The time representation of these viscoelastic functions is then obtained with the inverse Laplace transform. In order to assess the feasibility of this conversion method, it was applied to discrete data retrieved from the work of Schapery and Park [19]. The creep compliance $D(t)$ has been computed from the discrete valued source function $E(t)$. The verification process can be found in Appendix C.

4. Application to Finite Element generated data

Since the present work focuses on the verification of the methodology, no experimental data was processed. The identification procedure with the Laplace Virtual Fields Method was applied to data generated via Finite Element (FE) simulations. The implicit solver *Z-set* developed at ONERA and Mines Paris Tech was used [40]. An uniaxial tensile test was simulated on a double notched specimen geometry to generate heterogeneous kinematic fields. The isotropic linear viscoelastic constitutive relationship given by Equation (2) was used within a 2D plane stress hypothesis. The integration of this constitutive relationship was performed using a temporal implicit scheme. The time dependant moduli $K(t)$ and $G(t)$ were described with a Prony series implementation available in the *Z-mat* material library. The method was first applied on FE data to verify the proposed protocol. Then, random noise was applied to the FE data in order to evaluate the sensitivity to noise. The identified viscoelastic functions via the L-VFM have been compared with their analytical expressions from the Prony series.

4.1. Finite Element data generation

4.1.1. Reference constitutive model

The moduli $K(t)$ and $G(t)$ were defined with a generalized Maxwell model, which is mathematically defined in form of Prony series. This model expresses the time dependence of the moduli as

$$R(t) = R_0 - \sum_{n=1}^N R_n (1 - \exp(-t/\rho_n)) \quad (27)$$

with $R = \{K, G\}$ the moduli, the first term R_0 is the instantaneous elastic stiffness, the second term describes the delayed behaviour. The latter represents the temporal decay of the moduli as a sum of N terms describing the relaxation mechanisms (Figure 1b). Each relaxation mechanism is associated with a characteristic relaxation time ρ_n . Note that for a purely elastic material, the second term is zero, and the instantaneous elastic stiffness stays constant over time. Since the number and the values of the Prony series terms is not of matter here, a number of 4 arbitrary Prony series terms were used from the *Z-mat manual*. The characteristic relaxation times associated with the bulk and shear moduli are independent from one another. They are summarised in Table 1.

Table 1. Prony series parameters used for the simulations

K_0 [MPa]		G_0 [MPa]		
42261.90		29098.36		
n	K_n [MPa]	ρ_n^K [s]	G_n [MPa]	ρ_n^G [s]
1	8628.57	0.01	6692.62	0.43
2	2444.76	0.31	5528.69	9.07
3	1294.29	0.27	7856.56	27.62
4	16394.3	6.52	9020.49	102.86

4.1.2. Specimen geometry and simulation boundaries conditions

A double notched specimen was selected for the simulations (Figure 3a). The presence of the notches allows to generate heterogeneous strain fields from an uniaxial tensile test.

This geometry was meshed with linear 2D triangular elements using full integration within the plane stress framework, for a total of 4192 elements. An element size of 1 mm was chosen after a convergence study. The degrees of freedom of the bottom edge were blocked in the x_2 direction. For the upper edge, a displacement of 1 mm was imposed in the x_2 direction (Figure 3b). Concerning the x_1 direction, only the central nodes were blocked at the lower and upper edges.

In order to mimic real test conditions, the simulation was performed with a number of 200 evenly spaced time steps for a 20 seconds test. Thus, the simulation generated a database of 200 heterogeneous strain fields (Figure 3c). The force resultant from the upper boundary was also extracted. The viscous mechanisms due to the presence of the second term in Equation (27) can be observed as the load relaxes with time (Figure 3d). It should be noted that the time steps and the duration of the test have been arbitrarily chosen because significant viscoelasticity happens for this time scale and the considered Prony series coefficients. More generally, the time step and the duration of the test define the lower and upper limit of the observable time scale and would be defined accordingly to the test set-up and loading conditions.

4.1.3. Data interpolation

Images with 1024×1024 data points were created to represent a full-field measurement format. The strain components on that regular grid were computed based on the nodal displacements using the FE basis functions with Equation (28)

$$\varepsilon^{data} = B u^{nodes} \quad (28)$$

with ε^{data} the strain matrix on the regular grid, u^{nodes} the nodal FE displacements matrix, and B the matrix containing the derivatives of the element basis functions at the data points.

4.1.4. Noise application

Two data sets were generated. Firstly, in order to validate the methodology, no noise was added to the data. Then, zero mean Gaussian noise was added to the strains in order to have a first idea of the method sensitivity to noise. A standard deviation of $\lambda = 150 \mu\varepsilon$ was considered. The ratio between the maximum value and the standard deviation for each strain components are given in Table 2. These coefficients have been computed with

$$c_m = 100 \frac{\lambda}{\max(\varepsilon_{ij})} \quad (29)$$

where c_m is the ratio between the maximum value and the standard deviation expressed in percentage of the maximum value, λ the standard deviation and $\max(\varepsilon_{ij})$ the maximum strain value.

Table 2. Ratio between the maximum value and the standard deviation computed for each strain component. This ratio is expressed in percentage of the maximum value.

c_m	ε_{11} [%]	ε_{22} [%]	ε_{12} [%]
2.5	0.31	1	

The sensitivity study to noisy data is essential to assess the performance of the method for a real application. However, here, the noise was artificially added directly to the interpolated strain components. A study using a digital twin should be performed in a future work for a more realistic simulation [41].

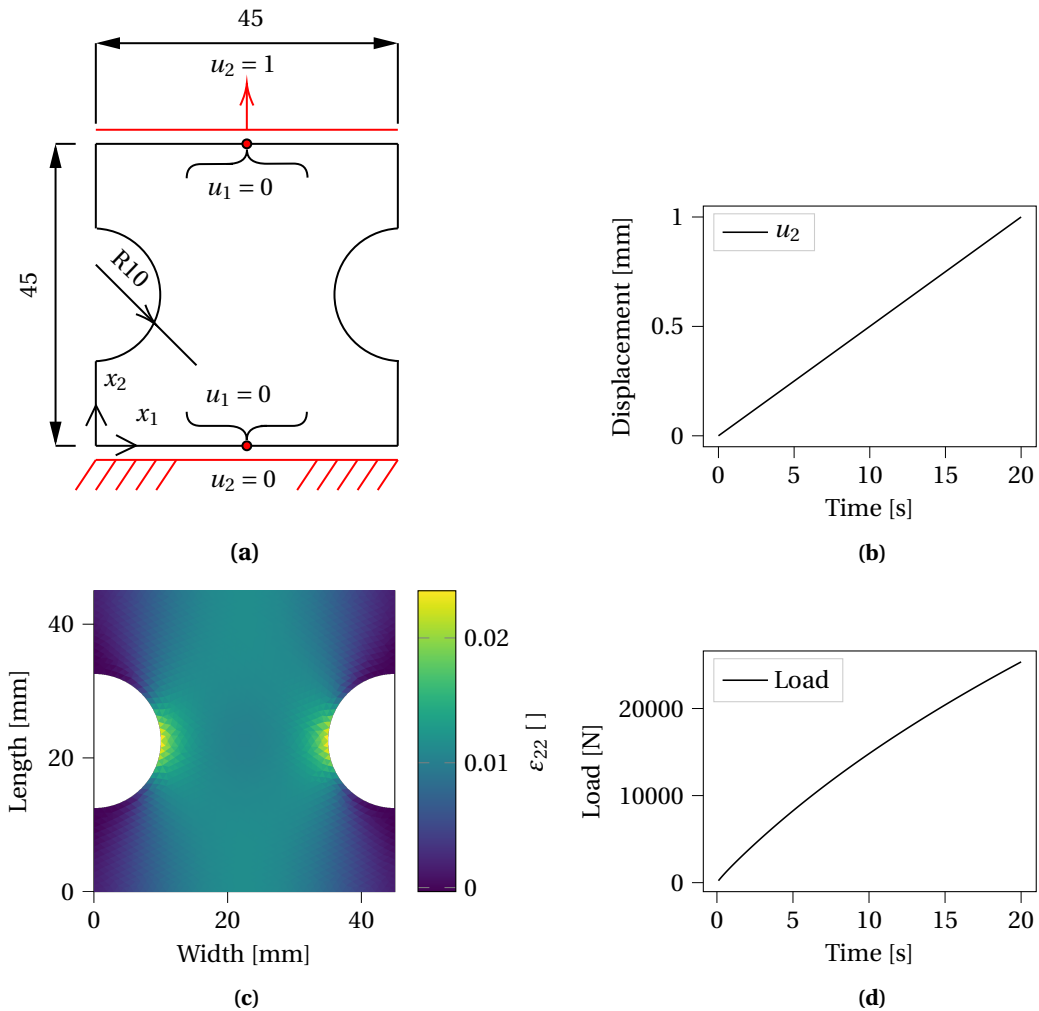


Figure 3. (a) Double notched specimen geometry used for the simulations, dimensions in mm. The degrees of freedom in the x_2 direction at the bottom edge were blocked. A displacement of 1 mm in the x_2 direction was imposed at the upper edge. For the x_1 direction, the displacements were blocked in the central node at the upper and lower edge. (b) Imposed displacement at the upper edge of the specimen. (c) strain map ε_{22} at time $t = 10$ s. The presence of the two notches generates a symmetrical heterogeneity. (d) Load evolution with time. The load relaxes with time as viscous mechanisms take place within the material.

4.2. Construction of the linear system in the Laplace domain

4.2.1. Virtual fields definition

Recalling the theoretical development made in Section 2, two virtual fields must be chosen to solve the problem. The virtual fields selection must fulfil three conditions for the method to be applied. In particular, the virtual fields must be :

- linearly independent,

- constant on the edges where the loading is applied, such that only the force resultant appears in the equations,
- constant in time.

In order to match these conditions, an arbitrary set of two fields were chosen for the present work

$$\begin{aligned}
 \text{Field n}^\circ 1 \quad \begin{cases} u_1^{*(1)} = (x_2 - L) x_2 x_1 \\ u_2^{*(1)} = 0 \end{cases} &\implies \begin{cases} \varepsilon_{11}^{*(1)} = (x_2 - L) x_2 \\ \varepsilon_{22}^{*(1)} = 0 \\ \varepsilon_{12}^{*(1)} = \frac{x_1 (2x_2 - L)}{2} \end{cases} \\
 \text{Field n}^\circ 2 \quad \begin{cases} u_1^{*(2)} = 0 \\ u_2^{*(2)} = x_2 \end{cases} &\implies \begin{cases} \varepsilon_{11}^{*(2)} = 0 \\ \varepsilon_{22}^{*(2)} = 1 \\ \varepsilon_{12}^{*(2)} = 0 \end{cases}
 \end{aligned} \tag{30}$$

The origin of the orthonormal basis was set to the lower left corner of the specimen (see Figure 3).

As an example, the virtual normal strain field $\varepsilon_{11}^{*(1)}$ obtained from the virtual field n°1 is presented in Figure 4. A greater weight is imposed at the center of the specimen where most of the heterogeneous information is concentrated (see Figure 3c).

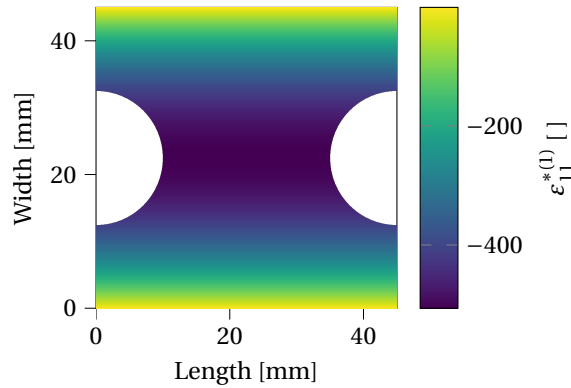


Figure 4. Virtual normal strain field $\varepsilon_{11}^{*(1)}$ obtained from the virtual field n°1.

4.2.2. Linear system construction

From the defined set of virtual fields, the discrete time description of the coefficients $A_{i1}(t)$, $A_{i2}(t)$, obtained from the virtual strains, and $B_i(t)$, obtained from the virtual displacements, were computed for each of the 200 time steps (Figure 5). The coefficients $A_{11}(t)$ and $A_{12}(t)$ obtained with the virtual field n°1 shows higher amplitude since a greater weight is imposed by the virtual strain on the real strains (see Figure 4). For the virtual field n°2, the virtual strain is constant so the coefficients $A_{21}(t)$ and $A_{22}(t)$ are the sum of the axial and lateral strains respectively (Figure 5a). For the loads, the virtual displacement n°1 cancels out the load imposed at the upper edge of the specimen such that $B(t)$ is 0. The virtual displacement n°2 is constant on the upper edge such that $B_2(t) = LF(t)$, with $F(t)$ the force resultant (Figure 5b).

The piecewise linear approximation and the Laplace transforms were applied to the different quantities using the formulation given in Appendix B. The linear system was built in the Laplace

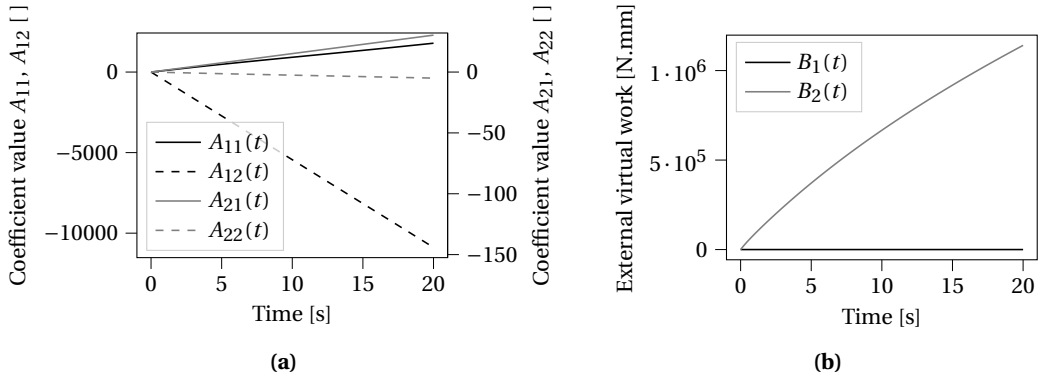


Figure 5. (a) Time evolution of the coefficients computed from the virtual strains. The coefficients $A_{11}(t)$ and $A_{12}(t)$ obtained from the first virtual strains are higher in amplitude because of the higher imposed weight by the virtual strains. The coefficients $A_{21}(t)$ and $A_{22}(t)$ obtained for the second virtual strain field are the sum of the respective axial and lateral strains. (b) Time evolution of the coefficients computed from the virtual displacements. Since the load is applied to the upper boundary of the specimen, the coefficient $B_1(t)$ and $B_2(t)$ are 0 and $LF(t)$ respectively, with $F(t)$ the force resultant.

domain and the matrix inversion was performed symbolically using Equation (23) such that the two following functions were obtained

$$\begin{cases} Q_{11}(s) = \frac{1}{s} \frac{-A_{12}(s)B_2(s)}{A_{11}(s)A_{22}(s) - A_{21}(s)A_{12}(s)} \\ Q_{12}(s) = \frac{1}{s} \frac{A_{11}(s)B_2(s)}{A_{11}(s)A_{22}(s) - A_{21}(s)A_{12}(s)} \end{cases} \quad (31)$$

The moduli $K(s)$, $G(s)$ and Poisson's ratio $\nu(s)$ were then expressed from Equation (31) in the Laplace domain following the relationships given by Equation (24). The values in the time domain were obtained through the inverse Laplace transform which evaluates the symbolical expressions of the built piecewise linear functions at each time step (see [27, 37]).

4.3. Results and discussion

The analytical values for Poisson's ratio and Young's modulus were obtained by conversion of the bulk and shear moduli using the Laplace and inverse Laplace transforms from their analytical expressions.

For the two cases the CME inversion algorithm was used with an order of 100^3 , since no significant improvement in the accuracy was obtained for higher order evaluations. The computation was performed on a laptop running with 8 Go RAM and an Intel Core i5-10210U CPU with a clock rate of 1.60 GHz. The results were obtained after 15 minutes⁴.

³The order is referred to as the number of evaluations of the function $F(s)$ for the computation of $f(t)$. More informations are available in [27, 37].

⁴Computational times may vary depending on the chosen order.

4.3.1. Results without noise

The identified and analytical moduli as well as Poisson's ratio over the time interval [0.1 s, 20 s] are provided in Figure 6. The results at time $t = 0$ s using the *initial value theorem* are given in Table 3.

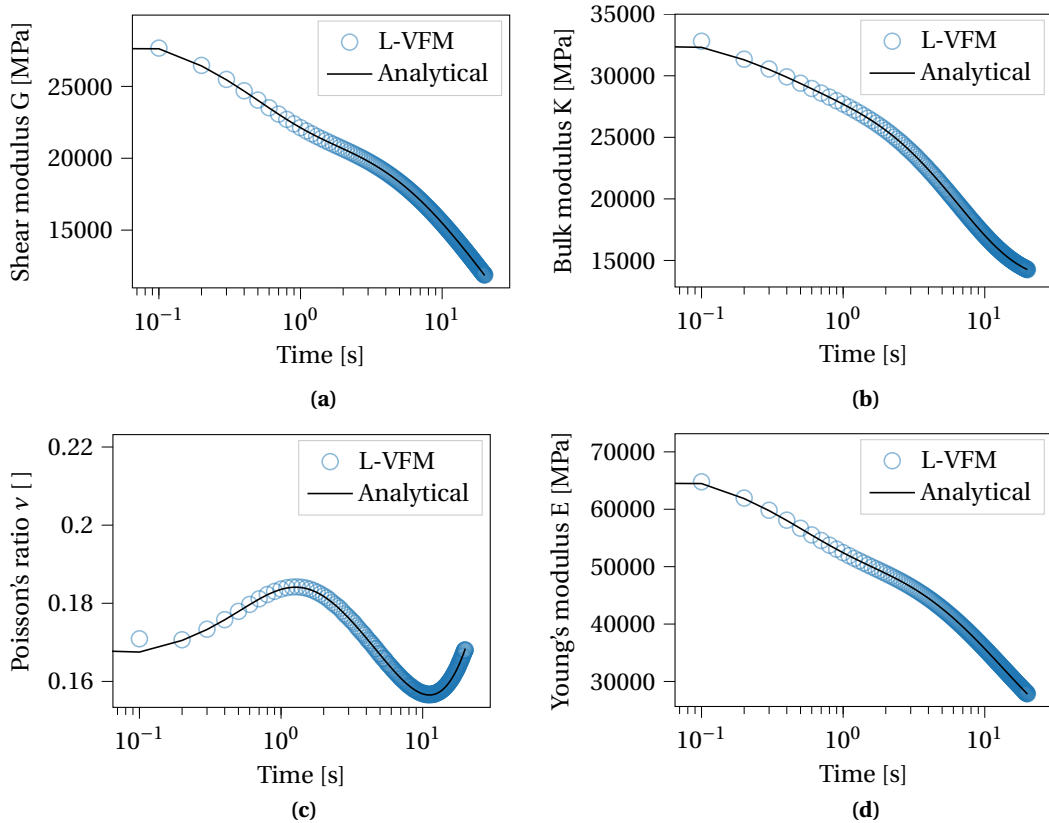


Figure 6. Comparison between the analytical and identified values using exact data for : (a), the shear modulus, (b), the bulk modulus, (c), Poisson's ratio, (d), Young's modulus. A good correspondence is observed between the identified and analytical viscoelastic functions. Nevertheless, the chosen time resolution of 0.1 s did not allow to capture the viscoelastic properties below 0.2 s.

Table 3. Identified vs reference values, exact data. The chosen time resolution was not sufficient to capture the relaxation mechanisms occurring during the first time step. The error is lower on G since slower relaxation mechanisms are used for the description of this parameter resulting in a lower sensitivity to the time resolution.

Parameter	K_0 [MPa]	G_0 [MPa]	ν_0 [-]	E_0 [MPa]
Analytical	42261.9	29098.36	0.22	71000
Identified (IVT)	33804.12	28332.21	0.17	66436
Error [%]	20	3	23	7

Globally, an excellent correspondence between the analytical and identified viscoelastic functions is observed. However, the identified values at time $t = 0$ s and $t = 0.1$ s are not consistent

with the analytical values. This is because the considered time resolution ($\Delta t = 0.1$ s), also known as the lower limit of the time scale [15], or sampling rate, was not sufficient to capture the relaxation mechanisms that takes place during the first time interval. From an another perspective, the time step $\Delta t = 0.1$ s acts like an upper cut-off frequency of 10 Hz. Considering the Nyquist theorem, the signal above 5 Hz can not be properly reconstructed ($\Delta t = 0.2$ s). Thus, the upper limits of the given Prony series model were not reached for this test (K_0, G_0). The effective modulus for the considered temporal resolution is the tangent modulus between the stresses and the strains, which is identified by the proposed method. In order for the tangent modulus to converge to the analytical values given by Equation (27), the time step Δt should be chosen such that only a purely elastic behavior happens within the first time interval. An illustrative example using a one-dimensional analytical model is given in Appendix D. In practice, this problem is well-known and one must define a time scale for which the viscoelastic behavior can be accurately observed. This time scale is impacted by two factors: the full-field measurement system framerate, and the temperature considered for the test since the time-temperature equivalence states that increasing or lowering the temperature of the sample is equivalent to respectively increase and decrease the lower limit of the timescale [15, 33].

If a large dataset was considered (i.e. a fine time step and/or a large time period), the computational cost of the method would increase as it would imply a larger number of pieces for the piecewise linear approximation of the A_{ij} and B_i coefficients (see Appendix B). This is because each pieces of the function is a local representation built at each time interval with independant heaviside and ramp functions. Thus, increasing the number of pieces is equivalent to increase the number of function evaluations in the inverse Laplace transform process. In order to reduce the computational cost, other functions could be used to approximate the coefficient A_{ij} and B_i , such as high order polynomials.

In order to assess the accuracy of the method, the mean absolute percentage error (MAPE) was computed with the following equation

$$\frac{100}{N_t} \sum_{t=0}^{N_t} \left| \frac{R - R_{id}}{R} \right| \quad (32)$$

where N_t is the number of temporal data points, R is the analytical value and R_{id} is the identified value. It was first computed for the time interval [0 s, 20 s] then considering the time interval [0.2 s, 20 s].

Table 4. Mean Absolute Percentage Error computed for the time interval [0 s, 20 s] and [0.2 s, 20 s] respectively. Due to the sampling rate of 0.1 s, the moduli and Poisson's ratio values below 0.2 s can not be accurately identified resulting in an increase of one order of magnitude in the error for K and ν due the fast relaxation mechanisms happening during the first time interval for these parameters. The impact is lower on the parameter G and E because of the slower relaxation mechanisms during the first time interval.

<i>MAPE</i>	<i>K</i> [%]	<i>G</i> [%]	ν [%]	<i>E</i> [%]
[0 s, 20 s]	0.15	0.028	0.18	0.045
[0.2 s, 20 s]	0.023	0.014	0.067	0.01

The results given in Table 4 shows that the error is an order of magnitude higher for K and ν for the [0 s, 20 s] time interval. This difference is lower for G since slower relaxations mechanisms are used for the description of this parameter (Table 1). The same observation is made for E . For the time interval of [0.2 s, 20 s] the MAPE displays an error with an order of $\pm 0.01\%$ for each viscoelastic function.

These results validate the proposed methodology, and show that the viscoelastic properties can be directly identified without any a priori parametrization of their time-dependance. Nevertheless, care must be taken for the timescale definition. If fast relaxation mechanisms happen for the considered material, the time resolution should be high enough to capture the viscoelastic properties with high accuracy. It should however be noted that this limitation is not specific to the L-VFM. It is just that the information is not present in the dataset.

4.3.2. Results with noise

The results with the introduction of noise are presented in Figure 7. From the discussion in Section 4.3.1, only the values over the time interval [0.2 s, 20 s] are considered. The MAPE was computed for each parameter. The results are given in Table 5.

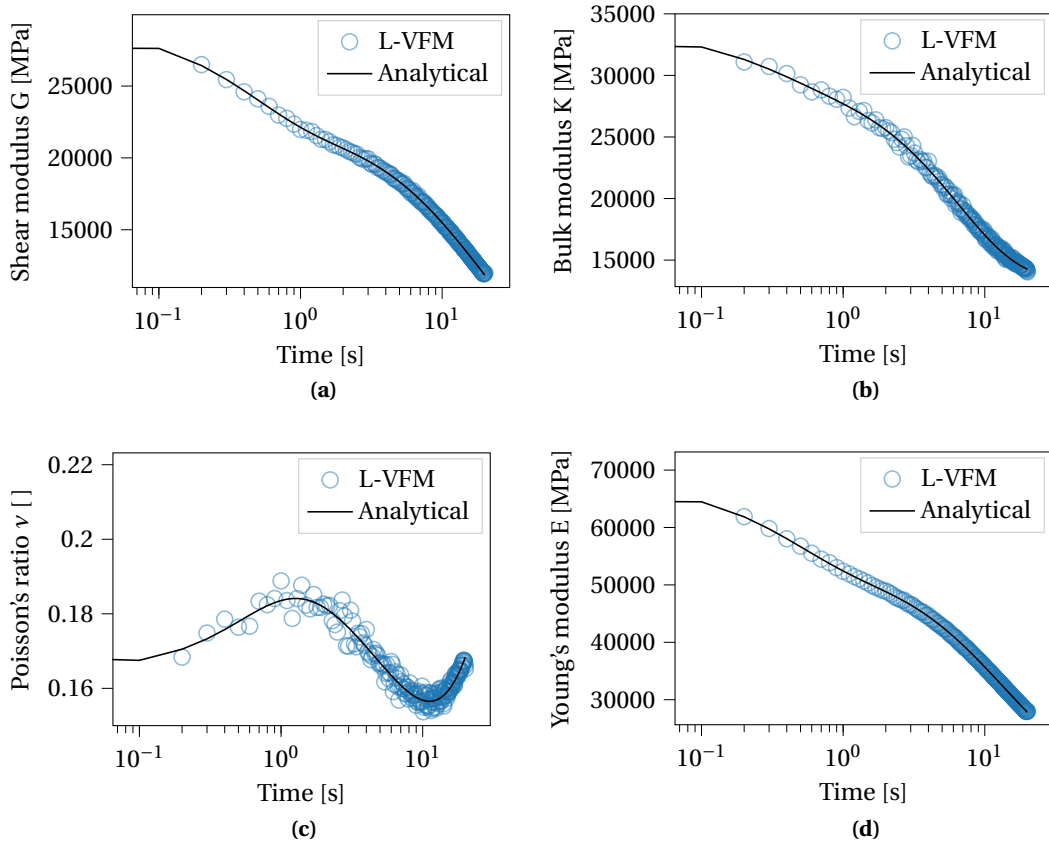


Figure 7. Comparison between the analytical and the identified values on the time interval [0.2 s, 20 s] considering a zero mean Gaussian noise with a 150 $\mu\epsilon$ standard deviation: (a), the shear modulus, (b), the bulk modulus, (c), Poisson's ratio and (d), Young's modulus. The noise sensitivity of the method is impacted by the convolution operations and the choice of the virtual fields. The impact of noise is higher at low time values because of the lower signal to noise ratio.

As usual, Poisson's ratio exhibits a higher sensitivity to noise as its impact on the mechanical fields is lower. The bulk modulus shows a higher noise sensitivity than the shear modulus and Young's modulus. This is because strains have been noised rather than displacements. The bulk

Table 5. Mean Absolute Percentage Error computed for the parameters identified from noisy strains. The error is an order of magnitude higher compared to the case where no noise was introduced, but still within 1% for all components, showing the stability of the L-VFM.

<i>MAPE</i>	<i>K</i> [%]	<i>G</i> [%]	ν [%]	<i>E</i> [%]
[0.2 s, 20 s]	0.73	0.23	0.8	0.13

modulus depends on two strain components while the shear modulus and Young's modulus only on one. If displacements had been noised, or even better, grey level images using the virtual twin described in [41], it is likely that this effect would have been less obvious.

The MAPE displays an error on the order of $\pm 0.1\%$ for each parameter. This is an order of magnitude higher compared to the case where no noise was introduced. The impact of noise is particularly important for the low time values. The low amplitude of the strain maps for these times leads to a lower signal-to-noise ratio (see Figure 8). However, the errors are still much lower than practical experimental uncertainties.

The noise sensitivity of the method is driven by two factors, the convolution operation and the choice of the virtual fields. Looking back at Equations (23) and (31), the matrix inversion is computed in the Laplace domain using the product of its components. Therefore, the frequency contents of the different signals are multiplied. This multiplicative operations in the complex frequency domain are equivalent to a convolution between the different noisy signals. For a deeper understanding of the impact of the convolution operation on the identified properties, future work considering a linear elastic model could be attempted. The elastic properties are constant in time. They can be identified via the linear Virtual Field Method and the Laplace Virtual Field Method. Therefore, the difference between the identified elastic properties using the two methods would only be due to the noise transmission through the Laplace and inverse Laplace transforms.

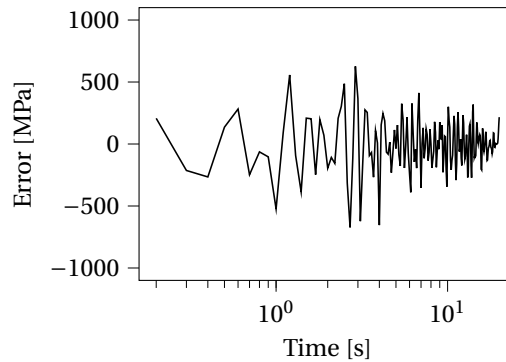


Figure 8. Error over time for the identified bulk modulus *K*, the impact of the noise is more important for low time values because of the lower signal to noise ratio

5. Conclusions and future works

A novel method based on the Virtual Fields Method and the Laplace transform has been developed. The Laplace formalism allows for a direct extraction of the viscoelastic properties of materials without any parametric modelling of their time-dependent behaviour. For a given temporally constant virtual field, the Laplace transform is applied to equilibrium equations through the principle of virtual work allowing to build up a linear system in the Laplace domain. This linear system is inverted, and a direct expression of the viscoelastic properties in the Laplace domain is obtained. The time representation of these viscoelastic properties is computed from their Laplace representation through the inverse Laplace transform. At first, the method has been validated by applying it to exact Finite Element generated data. Then, Gaussian noise was applied to the strains to simulate experimental data. This allowed for a first analysis of the noise sensitivity of the proposed methodology. The results showed that the viscoelastic properties can be directly identified using the proposed method. However, emphasis must be made on the different hypotheses and test conditions considered for the method implementation.

- (1) An isothermal test is considered in order for the viscoelastic functions to remain spatially homogeneous.
- (2) The temporal resolution is of important matter. If fast relaxation mechanisms happen for the considered material, a sufficiently fine time resolution is required to capture the viscous effect that could take place at low time values.
- (3) The virtual fields have been selected to be temporally constant, in order to express the constitutive model with its Laplace transform. This is probably not very restrictive in quasi-static as the viscoelasticity will not strongly affect the spatial distributions of strains. However, in inertial tests like the IBII test [33, 42] where spatial shapes follow wave propagation, this is likely to be a major limitation.

Future work will focus on experimental validation in static and at high strain rate, as well as the extension of the optimized virtual fields as defined in [43, 44] to this particular situation. A next step will also be to extend the method to orthotropic composites, particularly thermoplastic composites which exhibit significant viscoelasticity.

Conflicts of interest

The authors declare no competing financial interest.

Dedication

The manuscript was written through contributions of all authors. All authors have given approval to the final version of the manuscript.

CRedit authorship contribution statement

Quentin Marcot: Conceptualization, Methodology, Investigation, Software, Formal Analysis, Writing - Original Draft Preparation. **Thomas Fourest:** Conceptualization, Investigation, Software, Funding Acquisition, Supervision, Writing - Review & Editing. **Bertrand Langrand:** Conceptualization, Supervision, Funding Acquisition, Writing - Review & Editing. **Fabrice Pierron:** Conceptualization, Supervision, Funding Acquisition, Writing - Review & Editing.

Acknowledgments

The authors gratefully acknowledge the AID (French Ministry of Defense) for the funding of this work. The authors would also like to express their sincere gratitude to ONERA for providing all the necessary tools for the completion of this project.

Supplementary data

Supplementary material for this article is available on the open source escale platform at the following URL: https://gitlab.com/escale_team/escale. The data includes the programs used in this work and an example.

Appendix A. Equivalent elastic model in the Laplace domain

For a viscoelastic and isotropic material, the stress in the linear domain can be calculated using Equation (33)

$$\sigma_{ij}(t) = \int_0^t K(t-\tau) \dot{\varepsilon}_{kk}^V(\tau) \delta_{ij} d\tau + 2 \int_0^t G(t-\tau) \dot{\varepsilon}_{ij}^D(\tau) d\tau \quad (33)$$

where $K(t)$ and $G(t)$ are the bulk and shear moduli respectively, $\dot{\varepsilon}_{kk}^V \delta_{ij}$ and $\dot{\varepsilon}_{ij}^D$ are the volumetric and deviatoric strain rates respectively. Equation (33) uses two convolution operators, which can be written as

$$\sigma_{ij}(t) = K(t) \otimes \dot{\varepsilon}_{kk}^V \delta_{ij}(t) + 2G(t) \otimes \dot{\varepsilon}_{ij}^D(t) \quad (34)$$

where \otimes is the convolution operator. Applying the Laplace transform to Equation (34), the following expression is obtained

$$\mathcal{L}\{\sigma_{ij}(t)\} = \mathcal{L}\{K(t) \otimes \dot{\varepsilon}_{kk}^V \delta_{ij}(t) + 2G(t) \otimes \dot{\varepsilon}_{ij}^D(t)\} \quad (35)$$

where \mathcal{L} is the Laplace transform. Since the Laplace transform is a linear operator, the expression given by Equation (35) can be written as

$$\mathcal{L}\{\sigma_{ij}(t)\} = \mathcal{L}\{K(t) \otimes \dot{\varepsilon}_{kk}^V \delta_{ij}(t)\} + \mathcal{L}\{2G(t) \otimes \dot{\varepsilon}_{ij}^D(t)\} \quad (36)$$

Using the *convolution theorem*, the expression given by Equation (36) becomes

$$\underline{\underline{\sigma}}(s) = sK(s) \underline{\underline{\varepsilon}}_{kk}^V(s) + 2sG(s) \underline{\underline{\varepsilon}}_{ij}^D(s) \quad (37)$$

where s denotes the complex number associated with the Laplace transform. The expression given by Equation (37) can be written in a matrix formulation as given in Equation (38)

$$\underline{\underline{\sigma}}(s) = sK(s) \text{Tr}(\underline{\underline{\varepsilon}}(s)) \mathbb{1} + 2sG(s) \left(\underline{\underline{\varepsilon}}(s) - \frac{1}{3} \text{Tr}(\underline{\underline{\varepsilon}}(s)) \mathbb{1} \right) \quad (38)$$

Equation (38) can be reformulated as

$$\underline{\underline{\sigma}}(s) = \text{Tr}(\underline{\underline{\varepsilon}}(s)) \left(sK(s) - \frac{2}{3} sG(s) \right) \mathbb{1} + 2sG(s) \underline{\underline{\varepsilon}}(s) \quad (39)$$

The bulk and shear moduli $K(s)$ and $G(s)$ are then expressed as functions of the Young's modulus $E(s)$ Poisson's ratio $\nu(s)$ [4] with

$$K(s) = \frac{E(s)}{3[1-2\nu(s)]}; \quad G(s) = \frac{E(s)}{2[1+\nu(s)]} \quad (40)$$

Equation (39) can be rewritten as

$$\underline{\underline{\sigma}}(s) = \text{Tr}(\underline{\underline{\varepsilon}}(s)) \left(\frac{sE(s)}{3[1-2\nu(s)]} - \frac{sE(s)}{3[1+\nu(s)]} \right) \mathbb{1} + \frac{sE(s)}{[1+\nu(s)]} \underline{\underline{\varepsilon}}(s) \quad (41)$$

Taking the 2D plane stress hypothesis, such that

$$\sigma_{33}(s) = 0; \sigma_{13}(s) = 0; \sigma_{23}(s) = 0 \quad (42)$$

provides

$$\varepsilon_{33}(s) = -\frac{sv(s)}{1-sv(s)}(\varepsilon_{11}(s) + \varepsilon_{22}(s)); \varepsilon_{13}(s) = 0; \varepsilon_{23}(s) = 0 \quad (43)$$

Substituting the expression of $\varepsilon_{33}(s)$ from Equation (43) in the trace of the strain tensor $Tr(\underline{\underline{\varepsilon}}(s))$ in Equation (41) such that

$$Tr(\underline{\underline{\varepsilon}}(s)) = \varepsilon_{11}(s) + \varepsilon_{22}(s) + \varepsilon_{33}(s) = (\varepsilon_{11}(s) + \varepsilon_{22}(s)) \left(\frac{1-2sv(s)}{1-sv(s)} \right) \quad (44)$$

the following expression is obtained

$$\underline{\underline{\sigma}}(s) = \left(sv(s) \frac{sE(s)}{[1-(sv(s))^2]} \right) (\varepsilon_{11}(s) + \varepsilon_{22}(s)) \underline{\underline{1}} + \frac{sE(s)}{[1+sv(s)]} \underline{\underline{\varepsilon}}(s) \quad (45)$$

Equation (45) can be written as

$$\underline{\underline{\sigma}}(s) = \left(sv(s) \frac{sE(s)}{[1-(sv(s))^2]} \right) (\varepsilon_{11}(s) + \varepsilon_{22}(s)) \underline{\underline{1}} + \frac{sE(s)[1-sv(s)]}{[1-(sv(s))^2]} \underline{\underline{\varepsilon}}(s) \quad (46)$$

Equation (46) can be expressed using in-plane stiffness coefficients $Q_{11}(s)$ and $Q_{12}(s)$. In case of an isotropic material, these two coefficients are defined as

$$sQ_{11}(s) = \frac{sE(s)}{[1-(sv(s))^2]}; sQ_{12}(s) = sv(s) \frac{sE(s)}{[1-(sv(s))^2]} = sv(s)Q_{11}(s) \quad (47)$$

Substituting the expressions from Equation (47) into Equation (46), the following expression is obtained

$$\underline{\underline{\sigma}}(s) = sQ_{12}(s)(\varepsilon_{11}(s) + \varepsilon_{22}(s)) \underline{\underline{1}} + s(Q_{11}(s) - Q_{12}(s)) \underline{\underline{\varepsilon}}(s) \quad (48)$$

Due to the symmetry of the stress and strain tensors, the expression given by Equation (48) can be written in the Voigt formulation with

$$\underline{\underline{\sigma}}(s) = \begin{bmatrix} \sigma_{11}(s) \\ \sigma_{22}(s) \\ \sigma_{33}(s) \\ \sigma_{23}(s) \\ \sigma_{13}(s) \\ \sigma_{12}(s) \end{bmatrix}; \underline{\underline{\varepsilon}}(s) = \begin{bmatrix} \varepsilon_{11}(s) \\ \varepsilon_{22}(s) \\ \varepsilon_{33}(s) \\ 2\varepsilon_{23}(s) \\ 2\varepsilon_{13}(s) \\ 2\varepsilon_{12}(s) \end{bmatrix} \quad (49)$$

In the framework of 2D plane stress, and decomposing the strain tensor between its diagonal and non-diagonal values, Equation (48) can be written as

$$\begin{bmatrix} \sigma_{11}(s) \\ \sigma_{22}(s) \\ 0 \\ 0 \\ 0 \\ \sigma_{12}(s) \end{bmatrix} = sQ_{12}(s) \begin{bmatrix} \varepsilon_{11}(s) + \varepsilon_{22}(s) \\ \varepsilon_{11}(s) + \varepsilon_{22}(s) \\ \varepsilon_{11}(s) + \varepsilon_{22}(s) \\ 0 \\ 0 \\ 0 \end{bmatrix} + s(Q_{11}(s) - Q_{12}(s)) \begin{bmatrix} \varepsilon_{11}(s) \\ \varepsilon_{22}(s) \\ \varepsilon_{33}(s) \\ 0 \\ 0 \\ 0 \end{bmatrix} + s \frac{(Q_{11}(s) - Q_{12}(s))}{2} \begin{bmatrix} 0 \\ 0 \\ 0 \\ 0 \\ 0 \\ 2\varepsilon_{12}(s) \end{bmatrix} \quad (50)$$

Using the relationships $\varepsilon_{33}(s) = -\frac{s\nu(s)}{1-s\nu(s)}(\varepsilon_{11}(s) + \varepsilon_{22}(s))$ and $sQ_{12}(s) = s\nu(s)Q_{11}(s)$ from Equation (43) and (47) respectively, the third component from Equation (50) cancels out, and it can be rewritten as

$$\begin{bmatrix} \sigma_{11}(s) \\ \sigma_{22}(s) \\ \sigma_{12}(s) \end{bmatrix} = sQ_{12}(s) \begin{bmatrix} \varepsilon_{11}(s) + \varepsilon_{22}(s) \\ \varepsilon_{11}(s) + \varepsilon_{22}(s) \\ 0 \end{bmatrix} + s(Q_{11}(s) - Q_{12}(s)) \begin{bmatrix} \varepsilon_{11}(s) \\ \varepsilon_{22}(s) \\ 0 \end{bmatrix} + s \frac{(Q_{11}(s) - Q_{12}(s))}{2} \begin{bmatrix} 0 \\ 0 \\ 2\varepsilon_{12}(s) \end{bmatrix} \quad (51)$$

which gives

$$\begin{bmatrix} \sigma_{11}(s) \\ \sigma_{22}(s) \\ \sigma_{12}(s) \end{bmatrix} = sQ_{11}(s) \begin{bmatrix} \varepsilon_{11}(s) \\ \varepsilon_{22}(s) \\ 0 \end{bmatrix} + sQ_{12}(s) \begin{bmatrix} \varepsilon_{22}(s) \\ \varepsilon_{11}(s) \\ 0 \end{bmatrix} + s \frac{(Q_{11}(s) - Q_{12}(s))}{2} \begin{bmatrix} 0 \\ 0 \\ 2\varepsilon_{12}(s) \end{bmatrix} \quad (52)$$

and

$$\begin{bmatrix} \sigma_{11}(s) \\ \sigma_{22}(s) \\ \sigma_{12}(s) \end{bmatrix} = s \begin{bmatrix} Q_{11}(s) & Q_{12}(s) & 0 \\ Q_{12}(s) & Q_{11}(s) & 0 \\ 0 & 0 & \frac{Q_{11}(s) - Q_{12}(s)}{2} \end{bmatrix} \begin{bmatrix} \varepsilon_{11}(s) \\ \varepsilon_{22}(s) \\ 2\varepsilon_{12}(s) \end{bmatrix} \quad (53)$$

Appendix B. Piecewise-linear Laplace transform for discrete data

Let us assume that a function $f(t)$ can be represented by a piecewise-linear approximation. The interval $[0, T]$ is divided into $N_t - 1$ time intervals, where N_t is the number of time points. For each time segment Δt_i ($i = 0, \dots, N_t$), the piecewise linear approximation $p_i(t)$ of function $f_i(t)$ is expressed as a sum of step and ramp functions for $t_i \leq t \leq t_{i+1}$ and is zero for $t < t_i$ and $t > t_{i+1}$ [39].

$$p_i(t) = \begin{cases} 0, & \text{if } t < t_i \\ f(t_i)H(t - t_i) - f(t_{i+1})H(t - t_{i+1}) + \frac{\Delta f_i}{\Delta t_i} tH(t - t_i) - \frac{\Delta f_i}{\Delta t_i} tH(t - t_{i+1}), & \text{if } t_i \leq t \leq t_{i+1} \\ 0, & \text{if } t > t_{i+1} \end{cases} \quad (54)$$

where $H(t)$ is the Heaviside step function, $\Delta f_i = f_{i+1} - f_i$ and $\Delta t_i = t_{i+1} - t_i$. The Laplace transform of the Heaviside and ramp functions can be defined analytically from [34], such that

$$p_i(s) = \begin{cases} 0, & \text{if } t < t_i \\ \frac{f(t_i)}{s} \exp(-st_i) - \frac{f(t_{i+1})}{s} \exp(-st_{i+1}) + \frac{\Delta f_i}{s^2 \Delta t_i} [\exp(-st_i) - \exp(-st_{i+1})], & \text{if } t_i \leq t \leq t_{i+1} \\ 0, & \text{if } t > t_{i+1} \end{cases} \quad (55)$$

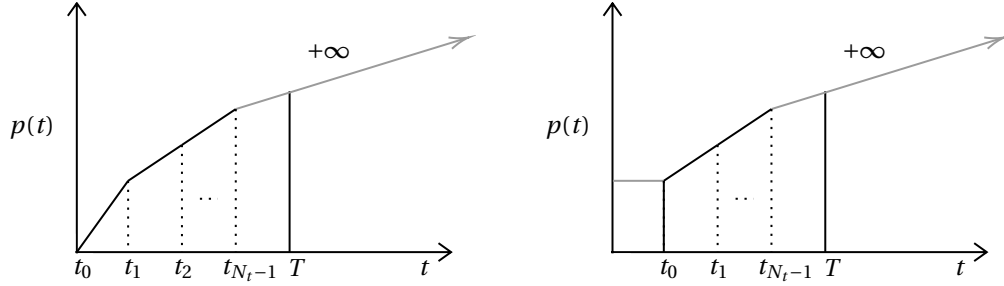
Equation (55) gives an analytical formulation for a piecewise linear approximation of discrete data over a time interval in the Laplace domain. The function $p(s)$ is expressed as the summation of the functions $p_i(s)$ over all $N_t - 1$ time intervals.

$$p(s) = \sum_{i=0}^{N_t-1} p_i(s) \quad (56)$$

From a numerical perspective, the evaluation of the input function $f(t)$ on a truncated segment $[0, T]$ is regarded as one period from the computation process, the function is only defined on the segment $[0, T]$. In order to avoid errors that could arise from this process, the ramp in the last time segment of the function $p(t)$ is extrapolated to $+\infty$, as shown in Figure 9a. If the function $f(t)$ is not initialised at time $t = 0$, its value a time $t = t_0 \neq 0$ is considered to be constant on between $t = 0$ and t_0 , as shown in Figure 9b.

The expression of the piecewise linear approximation $p(s)$ in the Laplace domain is given as

$$p(s) = \frac{f(t_0)}{s} [1 - \exp(-st_0)] + \sum_{i=0}^{N_t-2} p_i(s) + \frac{f(t_{N_t-1})}{s} \exp(-st_{N_t-1}) + \frac{\Delta f_{N_t-1}}{s^2 \Delta t_{N_t-1}} \exp(-st_{N_t-1}) \quad (57)$$



(a) Extrapolation of the last segment of the piecewise linear approximation $p(t)$ of function $f(t)$

(b) Extrapolation between the time segment $[0, t_0]$ of the piecewise linear approximation $p(t)$ for a function $f(t)$ that is not initialised at time $t = 0$ s

Figure 9. (a) Extrapolation of the last segment of the piecewise linear approximation $p(t)$ of function $f(t)$. (b) Extrapolation of the first time segment for a function $f(t)$ not initialized at time $t = 0$ s

Appendix C. Modulus interconversion using discrete data with the Laplace and inverse Laplace transforms

In order to validate the interconversion using a discrete approximation of the modulus function, it has been applied to raw data extracted from Schapery and Park [19]. In this paper, the authors introduce a method of interconversion using Prony series. With the proposed method, they are able to compute the creep compliance function $D(t)$ from the knowledge of the source relaxation modulus $E(t)$. Here the source function discrete data set was extracted and the creep compliance was computed using the Laplace transform of the discrete data set using the discrete approximation given in Appendix B. The creep compliance is related to the relaxation modulus in the Laplace domain through

$$D(s) = \frac{1}{s^2 E(s)} \quad (58)$$

The inverse Laplace transform was performed with the CME method for an order of 300 on the build function.

The results are given in Figure 10. A good correspondence is observed between the two methods, thus validating the applicability of this interconversion technique for the elastic constants from Equation (25).

Appendix D. Time step dependency of the tangent modulus

Let us assume a one dimensionnal linear visocelastic problem. The activated stress component can be computed using the one-dimensional convolution integral given by Equation (59).

$$\sigma(t) = \int_0^t R(t-\tau) \dot{\epsilon}(\tau) d\tau \quad (59)$$

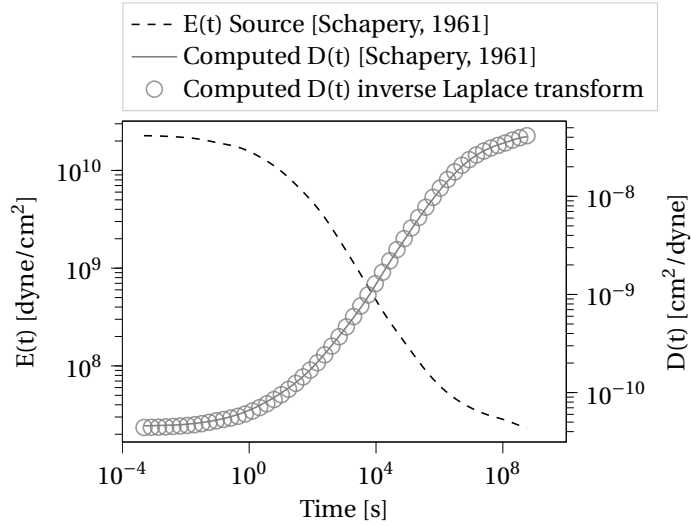


Figure 10. Comparison between the interconversion technique used by Schapery and Park [19] and the method using the Laplace and inverse Laplace transforms directly on the discrete data

with $R(t)$ the modulus and $\dot{\epsilon}$ the strain rate. Substituting $R(t)$ with a Prony series formulation (see equation (27)), the following equation is obtained

$$\sigma(t) = \int_0^t \left(R_0 - \sum_{n=1}^N R_n (1 - \exp(-(t-\tau)/\rho_n)) \right) \dot{\epsilon}(\tau) d\tau \quad (60)$$

Considering a constant strain rate, the following analytical expression is obtained (see [45])

$$\sigma(t) = \epsilon(t) \left(R_0 - \sum_{n=1}^N R_n \right) + \dot{\epsilon} \sum_{n=1}^N \rho_n R_n (1 - \exp(-t/\rho_n)) \quad (61)$$

From Equation (61) the tangent modulus can be computed using the following

$$R^{tan}(t) = \frac{d\sigma(t)}{d\epsilon(t)} \quad (62)$$

As an illustrative example, the Prony series terms in Equation (61) have been substituted with the bulk modulus values given in Table 1. The stress in Equation (61) has been computed for an arbitrary constant strain rate and a time of 20 seconds. Four time step values have been considered: $\Delta t = 0.001$ s and $\Delta t = 0.01$ s to simulate fast sampling rates, $\Delta t = 0.1$ s, which correspond to the time step chosen for the simulations and $\Delta t = 1$ s, to simulate a slow sampling rate. The tangent modulus has been computed numerically using a first order central finite difference scheme.

The results are given in Figure 11, the modulus values at time $t = 0$ s are given in Table 6. It is observed that increasing the sampling rate leads to the convergence of the tangent modulus to the analytical values, as stated in Section 4. In this case, for each sampling rate, the analytical values are reached for $t \geq 2\Delta t$. However, it should be noted that the frequency response of one order central finite differences does not reach a perfect response at the Nyquist frequency. Instead, such responses are generally reached at $f/4$ ($4\Delta t$) (see [46]).

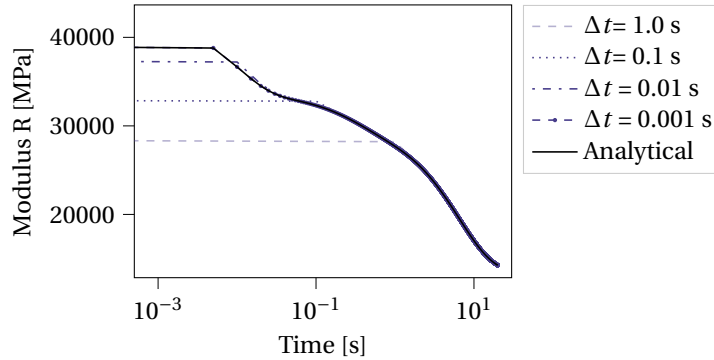


Figure 11. Analytical vs tangent modulus computed with a first order finite differences method for three time step values. Increasing the sampling rate induces a convergence of the tangent modulus to the analytical values as it allows to capture fast relaxation mechanisms. For each time step, the tangent modulus converges to the analytical values for $t \geq 2\Delta t$

Table 6. Analytical vs Tangent modulus at time $t = 0$ s.

R_0 [MPa]	42261.90			
Δt [s]	1	0.1	0.01	0.001
R_0^{tan} [MPa]	29852.22	33802.64	39012.29	41836.90

References

- [1] “ISO 899-1(en): Plastics — Determination of creep behaviour — Part 1: Tensile creep”, Standard, International Organization for Standardization, 2019.
- [2] “ISO 6271-1(en): Plastics — Determination of dynamic mechanical properties — Part 1: General principles”, Standard, International Organization for Standardization, 2019.
- [3] “ISO527-1(en): Plastics — Determination of tensile properties — Part 1: General principles”, Standard, International Organization for Standardization, 2019.
- [4] N. W. Tschoegl, W. G. Knauss, I. Emri, “Poisson’s Ratio in Linear Viscoelasticity – A Critical Review”, *Mech. Time Depend. Mater.* **6** (2002), no. 1, p. 3-51.
- [5] H. Schreier, J.-J. Orteu, M. A. Sutton, *Image Correlation for Shape, Motion and Deformation Measurements*, Springer, Boston, MA, 2009.
- [6] Y. Hoshino, K. Tamai, Y. Zhang, S. Yoneyama, “Direct measurement and master curve construction of viscoelastic Poisson’s ratio with digital image correlation”, *Strain* **54** (2018), no. 6, article no. e12294.
- [7] H. R. Cui, G. J. Tang, Z. B. Shen, “Study on the viscoelastic Poisson’s Ratio of Solid Propellants Using Digital Image Correlation Method”, *Propellants, Explos., Pyrotech.* **41** (2016), no. 5, p. 835-843.
- [8] J. Y. Choi, K. Yanamandra, A. Shetty, N. Gupta, “Simultaneous measurement of elastic constants from dynamic mechanical analysis with digital image correlation”, *Polymer* **242** (2022), article no. 124562.
- [9] S. Avril, M. Bonnet, A.-S. Bretelle, M. Grédiac, F. Hild, P. Lenny, F. Latourte, D. Lemosse, S. Pagano, E. Pagnacco, F. Pierron, “Overview of Identification Methods of Mechanical Parameters Based on Full-field Measurements”, *Exp. Mech.* **48** (2008), no. 4, p. 381-402.
- [10] M. Grédiac, F. Hild, *Full-Field Measurements and Identification in Solid Mechanics*, Mechanical Engineering and Solid Mechanics Series, ISTE; John Wiley & Sons, 2013.
- [11] F. Pierron, M. Grédiac, “Towards Material Testing 2.0. A review of test design for identification of constitutive parameters from full-field measurements”, *Strain* **57** (2020), no. 3, article no. e12370.
- [12] M. Grédiac, “Principe des travaux virtuels et identification”, *C. R. Acad. Sci., Paris, Série 2, Mécanique, Physique, Chimie, Sciences de l’univers, Sciences de la Terre* **309** (1989), no. 1, p. 1-5.
- [13] F. Pierron, M. Grédiac, *The Virtual Fields Method*, Springer New York, New York, NY, 2012.

- [14] R. Moulart, F. Pierron, S. R. Hallett, M. R. Wisnom, "Full-Field Strain Measurement and Identification of Composites Moduli at High Strain Rate with the Virtual Fields Method", *Exp. Mech.* **51** (2011), no. 4, p. 509-536.
- [15] S.-h. Yoon, C. R. Siviour, "Application of the Virtual Fields Method to a relaxation behaviour of rubbers", *J. Mech. Phys. Solids* **116** (2018), p. 416-431.
- [16] Y. Hoshino, Y. Zheng, S. Yoneyama, "Simultaneous Identification of Two-Independent Viscoelastic Characteristics with the Virtual Fields Method", in *Computational and Experimental Simulations in Engineering* (H. Okada, S. N. Atluri, eds.), Mechanisms and Machine Science, vol. 75, Springer, Cham, 2020, p. 11-20.
- [17] N. W. Tschoegl, *The Phenomenological Theory of Linear Viscoelastic Behavior: An Introduction*, Springer, Berlin Heidelberg, 1989.
- [18] J. Salençon, *Viscoelastic Modeling for Structural Analysis*, John Wiley & Sons, 2019.
- [19] S. W. Park, R. Schapery, "Methods of interconversion between linear viscoelastic material functions. Part I - A numerical method based on Prony series", *Int. J. Solids Struct.* **36** (1998), no. 11, p. 1653-1675.
- [20] R. A. Schapery, "A simple collocation method for fitting viscoelastic models to experimental data", Tech. Report 51778, Graduate Aeronautical Laboratory, California Institute of Technology, Pasadena, CA, 1962.
- [21] M. Lévesque, M. D. Gilchrist, N. Bouleau, K. Derrien, D. Baptiste, "Numerical inversion of the Laplace-Carson transform applied to homogenization of randomly reinforced linear viscoelastic media", *Comput. Mech.* **40** (2007), no. 4, p. 771-789.
- [22] S. Taguchi, K. Takeo, S. Yoneyama, "Computing Stresses from Measured In-plane Strains in Viscoelastic Body under Plane Stress Condition", *Adv. Exp. Mech.* **5** (2020), p. 135-140.
- [23] L. Boltzmann, "Zur Theorie der elastischen Nachwirkung", *Annalen der Physik und Chemie* **241** (1878), no. 11, p. 430-432.
- [24] R. A. Schapery, "Stress Analysis of Viscoelastic Composite Materials", *J. Compos. Mater.* **1** (1967), no. 3, p. 228-267.
- [25] J. D. Ferry, *Viscoelastic Properties of Polymers*, John Wiley & Sons, 1980.
- [26] P.-S. de Laplace, *Théorie analytique des probabilités*, Mme Ve Courcier, imprimeur-libraire pour les mathématiques et la marine, 57 quai des Augustins, 1812.
- [27] G. Horváth, I. Horváth, S. A.-D. Almousa, M. Telek, "Numerical inverse Laplace transformation using concentrated matrix exponential distributions", *Performance Evaluation* **137** (2020), article no. 102067.
- [28] N. W. Tschoegl, "Time Dependence in Material Properties: An Overview", *Mech. Time-Depend. Mater.* **1** (1997), no. 1, p. 3-31.
- [29] A. Marek, F. M. Davis, F. Pierron, "Sensitivity-based virtual fields for the non-linear Virtual Fields Method", *Comput. Mech.* **60** (2017), no. 3, p. 409-431.
- [30] T. Fourest, P. Bouda, L. C. Fletcher, D. Notta-Cuvier, E. Markiewicz, F. Pierron, B. Langrand, "Image-Based Inertial Impact test for characterisation of strain rate dependency of Ti6Al4V titanium alloy", *Exp. Mech.* **60** (2020), no. 2, p. 235-248.
- [31] A. Marek, F. M. Davis, M. Rossi, F. Pierron, "Extension of the sensitivity-based virtual fields to large deformation anisotropic plasticity", *Int. J. Mater. Form.* **12** (2019), no. 3, p. 457-476.
- [32] J.-D. Thoby, T. Fourest, B. Langrand, D. Notta-Cuvier, E. Markiewicz, "Robustness of specimen design criteria for identification of anisotropic mechanical behaviour from heterogeneous mechanical fields", *Computational Materials Science* **207** (2022), article no. 111260.
- [33] A. Matejunas, L. C. Fletcher, L. Lamberson, "An Image Based Inertial Impact test to extract viscoelastic constitutive parameters", in *36th Technical Conference of the American Society for Composites 2021: Composites Ingenuity Taking on Challenges in Environment-Energy-Economy* (O. Ochoa, ed.), Proceedings of the American Society for Composites, DEStech Publications, Inc., 2021, p. 904-913.
- [34] G. E. Roberts, H. Kaufman, *Table of Laplace transforms*, W. B. Saunders Company, 1966.
- [35] H. Inoue, M. Kamibayashi, K. Kishimoto, T. Shibuya, T. Koizumi, "Numerical Laplace Transformation and Inversion using Fast Fourier Transform", *J. Soc. Mech. Eng. Int. J. Ser. 1, Solid mechanics, strength of materials* **35** (1992), no. 3, p. 319-324.
- [36] J. Abate, W. Whitt, "A Unified Framework for Numerically Inverting Laplace Transforms", *INFORMS J. Comput.* **18** (2006), no. 4, p. 408-421.
- [37] J. Abate, G. L. Choudhury, W. Whitt, "An Introduction to Numerical Transform Inversion and Its Application to Probability Models", in *Computational Probability* (W. K. Grassmann, ed.), International Series in Operations Research & Management Science, vol. 24, Springer, Boston MA, 2000, p. 257-323.
- [38] D. P. Gaver, "Observing Stochastic Processes, and Approximate Transform Inversion", *Oper. Res.* **14** (1966), no. 3, p. 444-459.
- [39] P. Gómez, F. A. Uribe, "The numerical Laplace transform: An accurate technique for analyzing electromagnetic transients on power system devices", *Int. J. Electr. Power Energy Syst.* **31** (2009), no. 2-3, p. 116-123.
- [40] J.-D. Garaud, J. Rannou, C. Bovet, S. Feld-Payet, V. Chiaruttini, B. Marchand, L. Lacourt, V. A. Yastrebov, N. Osipov, S. Quilici, "Z-set -suite logicielle pour la simulation des matériaux et structures", in *14^e Colloque National en Calcul des Structures*, 2019.

- [41] M. Rossi, P. Lava, F. Pierron, D. Debruyne, M. Sasso, "Effect of DIC spatial resolution, noise and interpolation error on identification results with the VFM", *Strain* **51** (2015), no. 3, p. 206-222.
- [42] L. C. Fletcher, F. Pierron, "An Image-Based Inertial Impact (IBII) Test for Tungsten Carbide Cermets", *J. dynamic behavior mater.* **4** (2018), no. 4, p. 481-504.
- [43] M. Grédiac, E. Toussaint, F. Pierron, "Special virtual fields for the direct determination of material parameters with the Virtual Fields Method. 1 – Principle and definition", *Int. J. Solids Struct.* **39** (2002), no. 10, p. 2691-2705.
- [44] S. Avril, F. Pierron, "General framework for the identification of constitutive parameters from full-field measurements in linear elasticity", *Int. J. Solids Struct.* **44** (2007), no. 14, p. 4978-5002.
- [45] J. E. L. Pacheco, C. A. Bavastrri, J. T. Pereira, "Viscoelastic Relaxation Modulus Characterization Using Prony Series", *Lat. Am. J. Solids Struct.* **12** (2015), no. 2, p. 420-445.
- [46] I. R. Khan, R. Ohba, "New finite difference formulas for numerical differentiation", *J. Comput. Appl. Math.* **126** (2000), no. 1, p. 269-276.